Effect of blood rheological models on patient specific cardiovascular system simulations

Anastasios Skiadopoulos, Panagiotis Neofytou, and Christos Housiadas

***Abstract*—Newtonian and Quemada blood viscosity models are implemented in order to simulate the rheological behavior of blood under pulsating flow conditions in a patient specific iliac bifurcation. The influence of the applied blood constitutive equations is monitored via the Wall Shear Stress (WSS) distribution, magnitude and oscillations, non-Newtonian importance factors, and viscosity values according to the shear rate. The distribution of WSS on the vascular wall follows a pattern which is independent of the chosen rheological model. On the other hand, the WSS magnitude and oscillations are directly related to the applied blood constitutive equations and the shear rate. It is concluded that the Newtonian approximation may be regarded satisfactory only in high shear and flow rates.**

Keywords—blood flow simulation; patient specific; non-Newtonian models; wall shear stress; pulsating flow

I. Introduction

Blood flow in the cardiovascular system induces forces and stresses on the walls of the vessels which are closely related to the onset and localization of various diseases. Regions where low and oscillatory wall shear stresses develop are susceptible to the formation of atherosclerotic lesions [1-3]. This behavior is attributed to the non-uniformity of the vascular wall permeability [4]. Nerem, Mosberg and Schwerin [5] have demonstrated that the vascular wall permeability is directly related to the amplitude of the oscillatory shear stresses. Moreover, Fry [6] conducted experiments which proved that if the wall shear stresses are raised to high values for a short time, the endothelial surface may be damaged irreversibly. Furthermore, there is evidence that oscillating shear stresses on the arterial wall are related to the development and rupture risk of aortic aneurysms [7, 8].

Computational Fluid Dynamics (CFD) is a powerful tool which is widely applied for the simulation of blood flow in the cardiovascular system due to its non-intrusive nature. Commonly, blood is considered as a Newtonian fluid and vessels are idealized representations of the actual geometries. However, these modeling approximations may produce misleading results. The Newtonian fluid approximation ignores that blood viscosity depends on hematocrit and flow rate. The raise of the hematocrit increases blood viscosity. Moreover, it has been demonstrated that at low flow rates blood viscosity may be increased remarkably [9]. Additionally, the geometry of vessels plays a decisive role in the development of the flow field and the stresses on the wall. It is documented in the literature that atherosclerotic lesions tend to localize in areas where the geometry is complicated, such as branches and bifurcations [10, 11].

The goal of the present study is to investigate the influence of the geometry complexities and the blood constitutive equations in the magnitude and oscillation of WSS in patient specific blood flow simulations. A flow pulse is imposed at the inlet of the parent vessel of a patient specific iliac bifurcation for a time period of 0.8s, which corresponds to normal breathing conditions. The applied blood viscosity models are the Newtonian and Quemada [12]. The computational experiments reveal that there are significant differences in the WSS values between the two models, albeit a consistent WSS distribution pattern is present regardless of the applied model. The differences are more important at low flow rates indicating that the Newtonian model should be applied sparingly in patient specific blood flow simulations.

Manuscript received July 29, 2014.

A. Skiadopoulos (corresponding author, phone: +30 210 6503750; fax: +30 210 6545496; e-mail: tskiado@ipta.demokritos.gr), P. Neofytou (e-mail: panosn@ipta.demokritos.gr), and C. Housiadas (e-mail: christos@ipta.demokritos.gr) are with the Thermal Hydraulics & Multiphase Flow Laboratory, INRAESTES, NCSR "Demokritos", Agia Paraskevi, 15310, Greece.

II. Methods

A. Geometry Reconstruction

The original patient specific geometry is reconstructed from medical images in Digital Imaging and Communications in Medicine (DICOM) format via an in-house code [13]. Initially, the original medical imaging data are transformed into a triangulated surface in STereoLithography (STL) format by means of medical image visualization and slicing software. A multi-block structured grid that conforms to the triangulated surface is generated. Starting from the surface structured grid, the volume grid is generated in the interior of the domain. In the present study, a high quality, in terms of the elements skewness grid quality metric, multi-block structured grid was generated on an iliac bifurcation which was reconstructed from anonymous patient Computed Tomography (CT) data. The reconstructed geometry is depicted in Fig.1.

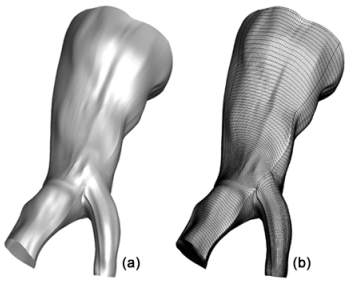

Fig. 1. View of the reconstructured surface (a) and the structured mesh (b).

B. Governing Equations

The physical problem is governed by the Navier-Stokes equations

$$\begin{aligned}
\frac{\partial}{\partial t}\int_\Omega \rho u d\Omega + \int_S \rho u \mathbf{V}\cdot d\mathbf{S} &= -\int_S p\mathbf{i}\cdot d\mathbf{S} + \int_S \left(\tau_{xx}\mathbf{i}+\tau_{xy}\mathbf{j}+\tau_{xz}\mathbf{k}\right)\cdot d\mathbf{S} \\
\frac{\partial}{\partial t}\int_\Omega \rho v d\Omega + \int_S \rho v \mathbf{V}\cdot d\mathbf{S} &= -\int_S p\mathbf{j}\cdot d\mathbf{S} + \int_S \left(\tau_{yx}\mathbf{i}+\tau_{yy}\mathbf{j}+\tau_{yz}\mathbf{k}\right)\cdot d\mathbf{S} \\
\frac{\partial}{\partial t}\int_\Omega \rho w d\Omega + \int_S \rho w \mathbf{V}\cdot d\mathbf{S} &= -\int_S p\mathbf{k}\cdot d\mathbf{S} + \int_S \left(\tau_{zx}\mathbf{i}+\tau_{zy}\mathbf{j}+\tau_{zz}\mathbf{k}\right)\cdot d\mathbf{S}
\end{aligned} \quad (1)$$

978-1-4799-7502-0/14 $31.00 © 2014 IEEE
DOI 10.1109/BIBE.2014.13

and the mass continuity equation

$$\int_S \mathbf{V} \cdot d\mathbf{S} = 0 \tag{2}$$

for three dimensional incompressible flow. In (1) and (2) $\mathbf{V} = [u, v, w]^T$ is the velocity vector with u, v and w representing the velocity components in x, y and z Cartesian coordinate respectively. Moreover, $d\mathbf{S}$ is equal to $\mathbf{n} \cdot dS$, where $\mathbf{n}$ is the unit vector normal to surface dS. In (1), $\mathbf{i}, \mathbf{j}$ and $\mathbf{k}$ are the unit vectors in x, y and z direction respectively, p is the pressure, ρ is the density, Ω is the volume of the domain, and τ_{ij} $(i, j = x, y, z)$ are the elements of the shear stress tensor.

The shear stresses τ_{ij} may be written in terms of the shear rate γ as

$$\tau_{ij} = \mu \gamma_{ij} \tag{3}$$

where μ is the molecular viscosity coefficient, which is constant in case of Newtonian flows and a function of the shear rate in non-Newtonian ones.

The shear rate may be written in tensorial form as

$$\bar{\boldsymbol{\gamma}} = 2\bar{\mathbf{D}} = \nabla \mathbf{V} + \nabla \mathbf{V}^T \tag{4}$$

where $\bar{\mathbf{D}}$ is the deformation tensor. Thus, (3) may also be written in the tensorial form

$$\bar{\boldsymbol{\tau}} = \mu \bar{\boldsymbol{\gamma}} \tag{5}$$

where $\bar{\boldsymbol{\tau}}$ is the shear stress tensor. Following the principle of material objectivity, i.e. μ must remain unchanged regardless of the frame of reference, the shear rate may be calculated by

$$\left|\bar{\boldsymbol{\gamma}}\right| = \sqrt{2\mathrm{tr}\left(\bar{\mathbf{D}}^2\right)} \tag{6}$$

Thus, when performing three dimensional numerical simulations any constitutive equation for non-Newtonian fluids should first be written in the form of

$$\tau = \mu(\gamma)\gamma \tag{7}$$

and then it may be expressed in the tensorial form

$$\bar{\boldsymbol{\tau}} = \mu\left(\left|\bar{\boldsymbol{\gamma}}\right|\right)\bar{\boldsymbol{\gamma}} \tag{8}.$$

In the present study, the non-Newtonian model of Quemada [12] is used. In this model, the effective viscosity is calculated by the formula

$$\mu\left(\left|\bar{\boldsymbol{\gamma}}\right|\right) = \mu_F \left(1 - \frac{1}{2}\frac{k_0 + k_\infty \sqrt{\left|\bar{\boldsymbol{\gamma}}\right| / \gamma_c}}{1 + \sqrt{\left|\bar{\boldsymbol{\gamma}}\right| / \gamma_c}}\phi\right)^{-2} \tag{9}$$

where μ_F is the viscosity of plasma, ϕ is the hematocrit, and k_0, k_∞ and γ_c are model parameters.

C. Boundary Conditions

A time varying parabolic velocity profile is applied at the inlet of the parent vessel of the iliac bifurcation for a typical cardiac cycle of 0.8s, which corresponds to normal breathing conditions. In Fig. 2 the velocity at the inlet of the iliac artery is plotted versus time. The vessel walls are considered rigid tubes and the no-slip boundary condition at the walls is applied when solving the Navier-Stokes equations.

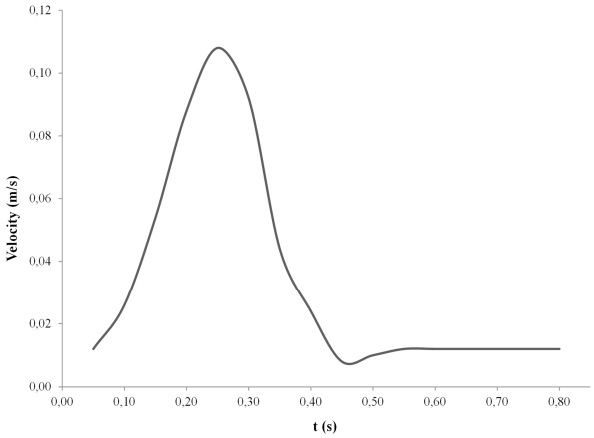

Fig. 2. Velocity waveform at the inlet.

At the bifurcation branches outlets, a predefined flow rate boundary condition is applied. At each time instance, the outflow rate of each branch is calculated as a fraction of the inflow based on the area of the outlet.

D. Haemodynamic parameters

In the Newtonian blood model the molecular viscosity coefficient remains constant. Its value in the performed numerical simulations is $\mu_\infty = 4 \cdot 10^{-3}$ Pa·s. The density of blood is ρ=1055 Kg/m^3.

For the Quemada model, the value of the plasma viscosity μ_F is $1.2 \cdot 10^{-3}$ Pa·s and the haematocrit is $\phi = 0.45$. The values of the model parameters are $k_0 = 4.33$, $k_\infty = 2.07$ and $\gamma_c = 1.88 s^{-1}$, corresponding to the selected value of the haematocrit [12].

E. Numerical Modelling

The mass continuity and Navier-Stokes equations are solved numerically using a parallel in-house CFD code [14, 15]. The code employs the Semi- Implicit Method for Pressure Linked Equations (SIMPLE) algorithm of [16] in conjunction with a finite-volume method (FVM) on multi-block, collocated, body-fitted 3D grids, where grid non-orthogonality is taken into account. The Navier-Stokes equations are discretized using a first-order forward Euler scheme for the time dependent term, a third-order QUICK scheme for the convective term and a central difference scheme (CDS) of second-order for the diffusion (viscous) term, whereas the pressure term is treated as source [17]. The solution is converged when the residual of the momentum and mass continuity is $1 \cdot 10^{-4}$.

The flow solver is parallelized via a domain decomposition technique which is based on the additive Schwarz method. Communication between processes is accomplished through the Message Passing Interface (MPI) message passing system, due to its high communication performance and portability. Numerical simulations were performed on a High Performance Computing (HPC) Rocks Cluster.

The $\mathbf{WSS}$ acting on the arterial wall is calculated by

$$\mathbf{WSS} = \mu \frac{\mathrm{d}\mathbf{V}_t}{\mathrm{d}\mathbf{r}_t} \tag{10}$$

where $\mathbf{r}_t$ and $\mathbf{V}_t$ are the direction vector and the velocity vector parallel to the arterial wall respectively.

In order to quantify the variation of the WSS on the arterial wall, the Area Averaged WSS $(AAWSS)$ variable is used. It is calculated by

$$AAWSS = \frac{1}{A_w} \sum_{i=1}^{n_w} \left|\mathbf{WSS}\right|_i \cdot S_{w_i} \tag{11}$$

where A_w is the total vascular wall area, n_w is the total number of the computational nodes lying on the wall, and S_{w_i} is the area of the wall face i.

The Area Averaged Shear Rate $(AASR)$ is used as a measure of the average shear rate on the arterial wall interface. It is calculated by the formula

$$AASR = \frac{1}{A_w} \sum_{i=1}^{n_w} \left|\bar{\boldsymbol{\gamma}}\right|_i \cdot S_{w_i} \tag{12}$$

where $\left|\bar{\boldsymbol{\gamma}}\right|_i$ is the shear rate at wall node i, calculated by (6).

The divergence of the non-Newtonian applied model from the Newtonian ,in terms of blood viscosity, is quantified by the global non-Newtonian importance factor I_G [18] which is calculated by the formula

$$I_G = \frac{1}{n_w} \frac{\left[\sum_{i=1}^{n_w} \left(\mu - \mu_\infty\right)^2\right]^2}{\mu_\infty} \tag{13}$$

The total WSS exerted on a node of the arterial wall over the entire cardiac cycle is evaluated by the Time Averaged WSS $(TAWSS)$

$$TAWSS = \frac{1}{T} \int_0^T \left|\mathbf{WSS}\right| \mathrm{d}t \tag{14}$$

where $\left|\mathbf{WSS}\right|$ is the magnitude of the instantaneous WSS vector, and T is the total duration of the cardiac cycle.

Similar to $AAWSS$, the TAS variable is introduced as a means of determining a total shear load on the vascular wall for the entire cardiac cycle. Its value is calculated by

$$TAS = \frac{1}{A_w} \sum_{i=1}^{n_w} TAWSS_i \cdot sw_i \tag{15}$$

where $TAWSS_i$ is the value of $TAWSS$ on wall node i.

The Oscillating Shear Index (OSI) is used as a means of determining the amplitude of the oscillations of the WSS on the arterial wall [1]. It is calculated by

$$OSI = 0.5 \left[1 - \frac{\left| \int_0^T \mathbf{WSS} \mathrm{d}t \right|}{\int_0^T \left|\mathbf{WSS}\right| \mathrm{d}t} \right] \tag{16}$$

The governing equations (1) and (2) are numerically solved in dimensionless form. Velocities, spatial coordinates and time are normalized by the peak systole velocity $U_{\max} = 0.108$ m/s, the diameter $D = 9.4 \cdot 10^{-3}$ m of the inlet of the parent vessel and the characteristic time $t_0 = D / U_{\max} = 8.7 \cdot 10^{-2}$ s respectively.

The Strouhal (Str) number is equal to $1.097 \cdot 10^{-1}$. For the Newtonian model the Reynolds (Re) number takes the value 270. For the Quemada model, the process of transforming the governing equations to dimensionless leads to the introduction of the dimensionless characteristic number Re_{Qu} [19], which is calculated by the formula

$$Re_{Qu} = \frac{\rho U_{\max} D}{\mu_F} \tag{17}$$

Based on the selected haemodynamic parameters, the value of Re_{Qu} for the performed numerical experiments is 900.

III. Results And Discussion

In Figs. 3 and 4 contour plots of the WSS on the arterial wall at peak systolic velocity for both models are presented. This characteristic time instance of the cardiac cycle is selected for demonstration purposes, since the velocity magnitude, and consequently the velocity gradients on the wall, obtain their maximum values.

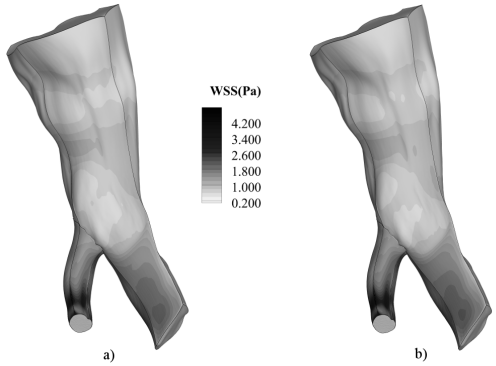

Fig. 3. WSS distribution on the arterial wall at peak systolic velocity. a) Newtonian, b) Quemada. Front view.

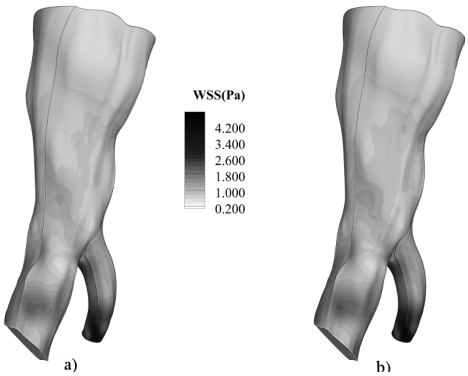

Fig. 4. WSS distribution on the arterial wall at peak systolic velocity. a) Newtonian, b) Quemada. Rear view.

It can be deduced from the contour plots that, regardless of the applied model, there is a consistent pattern of WSS distribution on the wall. Stresses are greater in value at places where the flow accelerates significantly, such as the outlet of the small branch of the bifurcation, or the vessel geometry presents acute curvature and creases. Albeit the WSS distribution is similar among the applied models, the stresses values differ significantly. In Table I the maximum values of the WSS acting on the vascular wall at characteristic time instances distributed over the entire cardiac cycle are recorded.

TABLE I. MAXIMUM VALUES OF WSS

t(s)	Maximum WSS (Pa)	
	Newtonian	*Quemada*
0.050	0.379	0.434
0.100	0.928	1.023
0.150	2.186	2.365
0.200	3.903	4.172
0.250	5.013	5.319
0.300	4.048	4.350
0.350	1.666	1.862
0.400	0.836	0.934
0.450	0.239	0.281
0.500	0.313	0.363
0.550	0.380	0.435
0.600	0.378	0.432
0.650	0.378	0.433
0.700	0.378	0.433
0.750	0.378	0.433
0.800	0.378	0.433

The Quemada model presents the maximum WSS value on the arterial wall throughout the cardiac cycle. The $AAWSS$ values, calculated by (11), provide an estimation of the WSS exerted on the entire wall surface. In Table II the values of $AAWSS$ for the same instances are recorded. In addition to the $AAWSS$ values, the difference in the calculated values between the applied models, weighted on the $AAWSS$ of the Quemada model, is recorded in Table II. Specifically, the weighted difference $\Delta AAWSS$ is calculated by

$$\Delta AAWSS = \frac{AAWSS_{Qu} - AAWSS_{Newt}}{AAWSS_{Qu}} \cdot 100 \qquad (18)$$

where $AAWSS_{Qu}$ and $AAWSS_{Newt}$ are the $AAWSS$ values for the Quemada and Newtonian model respectively.

TABLE II. AAWSS VALUES

t(s)	AAWSS (Pa)		ΔAAWSS (%)
	Newtonian	*Quemada*	
0.050	0.219	0.285	30.35%
0.100	0.592	0.700	18.19%
0.150	1.403	1.579	12.55%
0.200	2.496	2.749	10.15%
0.250	3.153	3.450	9.40%
0.300	2.496	2.747	10.06%
0.350	0.864	0.986	14.12%
0.400	0.385	0.461	19.74%
0.450	0.114	0.129	13.34%
0.500	0.155	0.215	38.57%
0.550	0.211	0.279	32.17%
0.600	0.206	0.272	32.10%
0.650	0.206	0.272	31.97%
0.700	0.206	0.272	32.09%
0.750	0.207	0.272	31.55%
0.800	0.207	0.273	31.64%

It can be directly inferred that as the flow accelerates the difference in the values of $AAWSS$ is reduced, reaching its minimum at peak systole. On the other hand, as the flow decelerates the difference in $AAWSS$ values is magnified. This behavior may be attributed to the fact that at very low flow rates blood viscosity increases notably [9].

In Table III the $AASR$ values along with the global non-Newtonian importance factor I_G, calculated by (12) and (13) respectively, are recorded. The values are computed for both applied models at the same time instances of the cardiac cycle. The I_G values indicate, as anticipated, that at low flow rates the non-Newtonian behavior of blood is prominent, whereas it fades at high flow rates. The results are consistent with experimental studies which prove that at shear rates above 100 s^{-1} the Newtonian fluid approximation for human blood is sufficient [20]. The $AASR$ values predicted by the two models are similar throughout the simulation period. From the onset of the systolic phase up to the mid-diastolic phase the Quemada

model predicts a higher average shear rate on the vascular wall, whereas the opposite occurs for the remainder of the cardiac cycle.

TABLE III. IG AND AASR VALUES

t(s)	AASR (s^{-1})		IG (%)
	Newtonian	*Quemada*	
0.050	54.692	54.591	14.00%
0.100	105.872	106.780	10.26%
0.150	204.967	206.729	7.60%
0.200	323.155	325.258	6.22%
0.250	394.335	396.412	5.69%
0.300	345.813	347.516	5.93%
0.350	188.444	188.698	7.54%
0.400	114.058	113.214	10.45%
0.450	52.823	49.118	13.68%
0.500	50.813	49.086	13.48%
0.550	56.377	55.515	13.18%
0.600	56.255	55.675	13.45%
0.650	56.054	55.624	13.58%
0.700	55.922	55.579	13.65%
0.750	55.844	55.552	13.68%
0.800	55.796	55.536	13.70%

The total shear load acting on the arterial wall over the entire cardiac cycle is quantified by means of the *TAWSS* variable, which is computed by (14). In Figs. 5 and 6 contour plots of the *TAWSS* on the vessel wall are drawn for both models. As previously observed for the WSS field, the distribution of *TAWSS* on the arterial wall is similar for both applied blood rheological models. The distribution pattern may be attributed to the geometry of the vessel and the way it influences the flow field. On the other hand, the WSS magnitude is attributed to the flow rate applied at the inlet, and consequently the magnitude of velocity gradients on the wall, and the constitutive equations of blood.

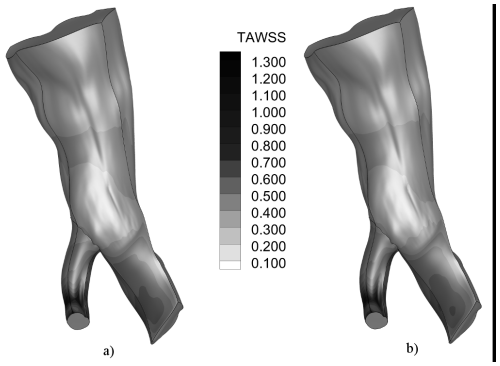

Fig. 5. TAWSS distribution on the arterial wall. a) Newtonian, b) Quemada. Front view.

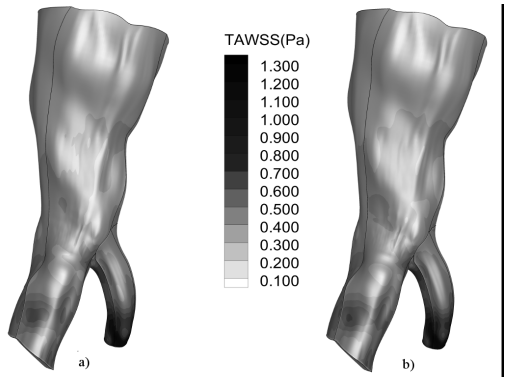

Fig. 6. TAWSS distribution on the arterial wall. a) Newtonian, b) Quemada. Rear view.

In Table IV the values of the *TAS* variable along with the maximum value of the *TAWSS* variable for both models are recorded. The percent difference in *TAS* values between the two models, weighted on the *TAS* value of the Quemada model, is 12.21 %.

TABLE IV. MAXIMUM VALUES OF TAWSS & TAS VALUES

Maximum TAWSS (Pa)		TAS (Pa)	
Newtonian	*Quemada*	*Newtonian*	*Quemada*
1.364	1.479	0.978	1.114

In Figs. 7 and 8 contour plots of the OSI index are drawn on the arterial wall for both the Newtonian and Quemada model. The OSI index, calculated by (16), is used as a measure of determining locations where the WSS values oscillate over a period of time The OSI value varies from 0 to 0.5. These values correspond to zero cyclic variation and 180^0 change of the WSS direction respectively. The maximum value of the OSI index is 0.482 and 0.472 for the Newtonian and Quemada model respectively. Examining the contour plots of the index together with the contour plots of the *TAWSS* , it can be directly deduced that the oscillations of the WSS are maximum at locations where the respective value is minor.

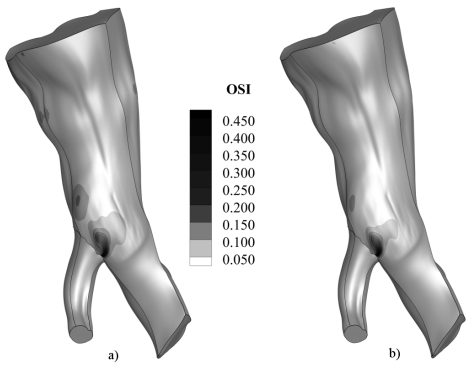

Fig. 7. OSI distribution on the arterial wall. a) Newtonian, b) Quemada. Front view.

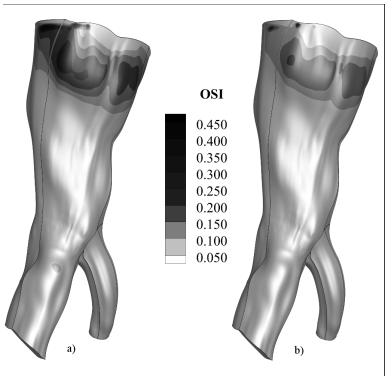

Fig. 8. OSI distribution on the arterial wall. a) Newtonian, b) Quemada. Rear view.

The regions of the arterial wall where the WSS are low and oscillatory have been documented to be more susceptible to the formation of atherosclerotic lesions [1-3] and more prone to the development of aneurysms [7, 8]. Comparison of the index value distribution between the two applied models leads to the conclusion that the Newtonian model over predicts areas where the WSS oscillates over time.

IV. Conclusion

The purpose of this work was to investigate the effect of blood rheological models on the magnitude, distribution and oscillation of WSS on the wall of a patient specific iliac bifurcation under pulsating flow conditions. The viscosity models applied were the Newtonian and Quemada in order to identify the limitations of the commonly used Newtonian fluid approximation in the context of blood flow simulations in the cardiovascular system.

The numerical experiments indicate that the stresses magnitudes are distributed on the arterial wall in a similar way regardless of the applied blood constitutive equations. However, both their area averaged values and the values at respective locations differ. The difference is significant at low flow rates and diminishes at high flow rates, with the Quemada model presenting always the higher stress value. Specifically, at peak systole the average stress value of the Quemada model is only 9.40% higher, whereas at $t = 0.5$ the difference in values is 38.57%. The area averaged shear value difference integrated over the entire cardiac cycle is 12.21%.

The non-Newtonian behavior of blood at low flow rates is verified by the values of the global non-Newtonian importance factors. At peak systole the average viscosity of blood for the Quemada model is 5.69% higher than the constant viscosity of the Newtonian model. The highest divergence in average viscosity values is observed at the onset of the cardiac cycle reaching the value of 13.70%.

Oscillations of the WSS are maximized at locations where their magnitudes are low for both models. The Newtonian model forecasts a wider area of the arterial wall on which the shear stresses oscillate.

Overall, it is concluded that the Newtonian fluid approximation may be considered sufficient only at high flow rates and, consequently, shear rates. At shear rates below the threshold of $100\,s^{-1}$ the non-Newtonian behavior of blood cannot be ignored and the implementation of the Newtonian model may lead to misleading results.

Accuracy of the simulations will be further enhanced with the introduction of the fluid structure interaction in the computations and the application of more physiologically realistic boundary conditions, which take into account the interaction with the upstream and downstream vasculature. In the future, simulation results will be compared to clinical data.

Acknowledgment

This work was financially supported by the National Strategic Reference Framework (NSRF) 2007-2013 project DEKA: ‘Integrated prognostic system for risk assessment in stent implantations for Abdominal Aortic Aneurysm repair’ (Code Number: 09ΣΥΝ-12-1153).

References

[1] D. N. Ku, D. P. Giddens, C. K. Zarins, and S. Glagov, "Pulsatile flow and atherosclerosis in the human carotid bifurcation. Positive correlation between plaque location and low and oscillating shear stress," *Arteriosclerosis,* vol. 5, pp. 293-302, 1985.

[2] C. Cheng, D. Tempel, R. Van Haperen, A. Van Der Baan, F. Grosveld, M. J. A. P. Daemen*, et al.*, "Atherosclerotic lesion size and vulnerability are determined by patterns of fluid shear stress," *Circulation,* vol. 113, pp. 2744-2753, 2006.

[3] E. Cecchi, C. Giglioli, S. Valente, C. Lazzeri, G. F. Gensini, R. Abbate*, et al.*, "Role of hemodynamic shear stress in cardiovascular disease," *Atherosclerosis,* vol. 214, pp. 249-256, 2011.

[4] S. Charm and G. Kurland, "Viscometry of Human Blood for Shear Rates of 0-100,000 sec-1," *Nature,* vol. 206, pp. 617-618, 05/08/print 1965.

[5] R. M. Nerem, A. T. Mosberg, and W. D. Schwerin, "Transendothelial transport of 131I albumin," *Biorheology,* vol. 13, pp. 71-77, 1976.

[6] D. L. Fry, "Acute Vascular Endothelial Changes Associated with Increased Blood Velocity Gradients," *Circulation Research,* vol. 22, pp. 165-197, 1968.

[7] Y. Hoi, H. Meng, S. H. Woodward, B. R. Bendok, R. A. Hanel, L. R. Guterman*, et al.*, "Effects of arterial geometry on aneurysm growth: three-dimensional computational fluid dynamics study," *Journal of Neurosurgery,* vol. 101, pp. 676-681, 2004/10/01 2004.

[8] M. L. Raghavan, B. Ma, and R. E. Harbaugh, "Quantified aneurysm shape and rupture risk," *Journal of Neurosurgery,* vol. 102, pp. 355-362, 2005.

[9] G. B. Thurston, "Viscoelasticity of human blood," *Biophysical Journal,* vol. 12, pp. 1205-1217, 1972.

[10] D. N. Ku, "Blood flow in arteries," in *Annual Review of Fluid Mechanics* vol. 29, ed, 1997, pp. 399-434.

[11] A. Wahle, J. J. Lopez, M. E. Olszewski, S. C. Vigmostad, K. B. Chandran, J. D. Rossen*, et al.*, "Plaque development, vessel curvature, and wall shear stress in coronary arteries assessed by X-ray angiography and intravascular ultrasound," *Medical Image Analysis,* vol. 10, pp. 615-631, 2006.

[12] D. Quemada, "Rheology of concentrated disperse systems III. General features of the proposed non-newtonian model. Comparison with experimental data," *Rheologica Acta,* vol. 17, pp. 643-653, 1978.

[13] E. Makris, P. Neofytou, S. Tsangaris, and C. Housiadas, "A novel method for the generation of multi-block computational structured grids from medical imaging of arterial bifurcations," *Medical Engineering & Physics,* vol. 34, pp. 1157-1166, 2012.

[14] P. Neofytou and S. Tsangaris, "Flow effects of blood constitutive equations in 3D models of vascular anomalies," *International Journal for Numerical Methods in Fluids,* vol. 51, pp. 489-510, 2006.

[15] P. Neofytou, S. Tsangaris, and M. Kyriakidis, "Vascular wall flow-induced forces in a progressively enlarged aneurysm model," *Computer*

Methods in Biomechanics and Biomedical Engineering, vol. 11, pp. 615-626, 2013/07/16 2008.
[16] S. V. Patankar, *Numerical Heat Transfer and Fluid Flow*, 2nd ed. New York: Hemisphere Publishing Co., 1996.
[17] J. H. Ferziger, Peric, M., *Computational Methods for Fluid Dynamics*, 3rd ed.: Springer, 2002.
[18] B. M. Johnston, P. R. Johnston, S. Corney, and D. Kilpatrick, "Non-Newtonian blood flow in human right coronary arteries: Steady state simulations," *Journal of Biomechanics,* vol. 37, pp. 709-720, 2004.
[19] P. Neofytou and D. Drikakis, "Effects of blood models on flows through a stenosis," *International Journal for Numerical Methods in Fluids,* vol. 43, pp. 597-635, 2003.
[20] T. J. Pedley, *The Fluid Mechanics of Large Blood Vessels*: Cambridge University Press, 1980.